



HAL
open science

Shedding Light on the Hidden Roles of Lithium in the Nickel-Catalyzed Cross-Coupling of Aryl Ethers

Haosheng Liang, Andryj Borys, Eva Hevia, Marie-Eve Perrin, Pierre-Adrien Payard

► **To cite this version:**

Haosheng Liang, Andryj Borys, Eva Hevia, Marie-Eve Perrin, Pierre-Adrien Payard. Shedding Light on the Hidden Roles of Lithium in the Nickel-Catalyzed Cross-Coupling of Aryl Ethers. *Journal of the American Chemical Society*, 2023, 145 (36), pp.19989-19999. 10.1021/jacs.3c06647 . hal-04285601

HAL Id: hal-04285601

<https://hal.science/hal-04285601>

Submitted on 14 Nov 2023

HAL is a multi-disciplinary open access archive for the deposit and dissemination of scientific research documents, whether they are published or not. The documents may come from teaching and research institutions in France or abroad, or from public or private research centers.

L'archive ouverte pluridisciplinaire **HAL**, est destinée au dépôt et à la diffusion de documents scientifiques de niveau recherche, publiés ou non, émanant des établissements d'enseignement et de recherche français ou étrangers, des laboratoires publics ou privés.

Shedding Light on the Hidden Roles of Lithium in the Nickel-Catalyzed Cross-Coupling of Aryl Ethers

Haosheng Liang,^{a,‡} Andryj M. Borys,^{b,‡} Eva Hevia,^{b*} Marie-Eve L. Perrin,^{a*} Pierre-Adrien Payard^{a*}

^a Université de Lyon, Université Claude Bernard Lyon I, CNRS, INSA, CPE, UMR 5246, ICBMS, Rue Victor Grignard, F-69622 Villeurbanne Cedex, France

^b Departement für Chemie, Biochemie und Pharmazie, Universität Bern, Bern 3012, Switzerland.

[‡] These authors contributed equally to this work.

KEYWORDS. Nickel, Catalysis, Cross-Coupling, Mechanism, Heterobimetallics, DFT

ABSTRACT: The Ni-catalyzed cross-coupling of aryl ethers is a powerful synthetic tool to transform widely available phenol derivatives into functionalized aromatic molecules. Recent theoretical and experimental mechanistic studies have identified the involvement of heterobimetallic nickelates as key intermediates that facilitate the challenging transformation under mild conditions, and often without the need for external ligands or additives. In this work, based on calculations performed at the DFT level and by comparison with spectroscopic and kinetic data, we investigate the mechanism of the Ni(COD)₂ catalyzed cross-coupling of 2-methoxynaphthalene with PhLi, and assess the speciation of lithium nickelate intermediates. The crucial role of solvent on the reaction is explained and the multiple roles played by lithium are unveiled. Experimental studies have identified key lithium nickelate species which support and help evolve the calculated reaction mechanism, and ultimately complete the catalytic cycle. Based on this new mechanistic knowledge, a well-known experimental challenge of these transformations, the so-called “naphthalene problem” which restricts the use of electrophilic coupling partners to π -extended systems, can be addressed to enable the cross-coupling of unbiased aryl ethers under mild conditions.

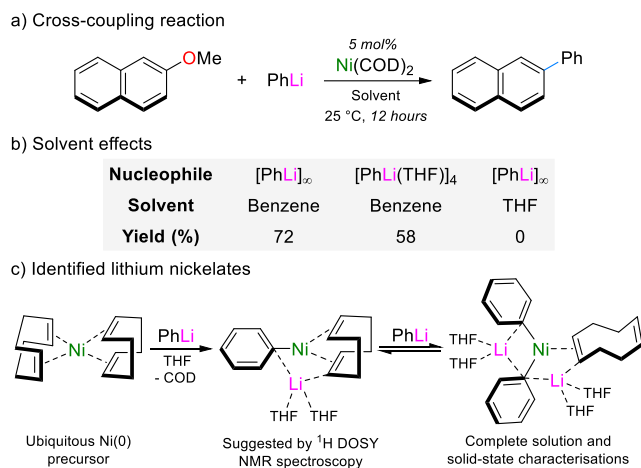
INTRODUCTION

The selective cleavage of C–O bonds and subsequent functionalization by transition-metal-catalyzed cross-coupling reactions constitutes an attractive strategy for the direct valorization of widely available phenol derivatives.^{1–3} Etheral C–O bonds are rather unreactive however, and most of the well-established Pd-catalyzed cross-coupling methods are generally ineffective for these challenging substrates. Ni-catalysis, on the other hand, has proven to be powerful for many types of C–O bond functionalization reactions, including the cross-coupling and hydrogenolysis of aryl ethers.^{4,5} As early as 1979, Wenkert reported the first Ni-catalyzed activation of inert C_{aryl}–OMe bonds in a Kumada-Tamao-Corriu type cross-coupling reaction.⁶ In more recent years, aryl ether derivatives have been used as electrophilic coupling partners in several types of cross-coupling reactions, including Suzuki, Negishi and Murahashi.⁴ Nevertheless, the range of aryl ethers that can be activated under these conditions is still quite limited, although the use of specific ligands or nucleophiles has helped overcome this so-called “naphthalene problem”.^{7–10} For cross-coupling reactions involving aryl ethers, the choice of solvent, ligand and nucleophilic coupling partner have proven to be crucial, but mechanistic details on how these reactions proceed is still rather limited.⁵

The conventional mechanism of cross-coupling reactions starts from a neutral Ni⁰ complex and involves three key steps: (i) oxidative addition of the C–X bond to a ligated Ni⁰ center; (ii) transmetalation between the organometallic nucleophile and the Ni^{II} complex; and (iii) reductive elimination between the

organic substituents to deliver the cross-coupled product and regenerate Ni⁰.¹¹ Based on both experimental and computational mechanistic studies however, this simplified mechanism has been shown to be inappropriate for aryl ethers due to the high bond dissociation enthalpy of the C_{aryl}–OMe bond.⁵ DFT calculations by Wang and Uchiyama provided support for an alternative *anionic pathway* which instead involve anionic nickelate intermediates.^{12–14} Nevertheless, the lack of experimental evidence, the use of a simplified chemical model and the limited speciation of both nickelate complexes and polar organometallic aggregates temper the conclusions drawn.

More recently, our group has provided an in-depth experimental mechanistic study into the cross-coupling reaction between 2-methoxynaphthalene and phenyl-lithium catalyzed by Ni(COD)₂ (where COD = 1,5-cyclooctadiene) (**Scheme 1**).¹⁵ The co-complexation of Ni(COD)₂ with PhLi gives rise to two different heterobimetallic nickelates; a 1:1 species [Li(THF)₂PhNi(COD)_n] (where n = 1 or 2) and a 2:1 species [Li₂(THF)₄Ph₂Ni(COD)], which were found to exist in equilibria. Stoichiometric, catalytic and kinetic studies support the involvement of these lithium nickelates in the cross-coupling reaction, but precise details on how they facilitate the C–OMe bond cleavage were still unclear. Notably, the cross-coupling reaction has a strong solvent and donor influence, suggesting that Li and Ni work cooperatively to enable the transformation under mild conditions.¹⁵



Scheme 1. a) Cross-coupling reaction between 2-methoxynaphthalene and PhLi catalyzed by Ni(COD)₂. b) Influence of solvent on the yield of 2-phenylnaphthalene. c) Identified lithium nickelates derived from Ni(COD)₂ and PhLi.

In this work, based on calculations performed at the DFT level and by comparison with spectroscopic and kinetic data, we clarify the nature (stoichiometry and ligands) of the active lithium nickelate complexes formed under catalytic reaction conditions. The crucial role of solvent on the reaction are explained and the multiple roles played by lithium are evidenced. Further stoichiometric reactions have identified additional nickelate intermediates which offer further support for the calculated mechanism. Based on this new mechanistic knowledge, we also demonstrate how the “naphthalene problem” can be overcome to enable the cross-coupling of unbiased aryl ethers under mild conditions.

COMPUTATIONAL DETAILS

All calculations were performed at the DFT level using the Gaussian 09 (Rev D.01) suite of programs.¹⁶ The speciation of PhLi(THF)_n and Ni(COD)₂ in THF was first considered to benchmark the computational method and to define the reference state of the catalytic system (see the SI for further details). Structure of minima and transition states were fully optimized using the M06 DFT functional,¹⁷ this functional shows good performance to predict the structure and energy of organonickel complexes.¹⁸ First to third period atoms (C, H, Li, and O) were described using the double- ζ Karlsruhe basis sets (def2-SVP).^{19,20} The fully relativistic effective-core potential (ECP10MDF)²¹ from the Stuttgart/Köln group and its associated basis set²² was used to describe Ni. Bulk solvent effects were represented using the SMD implicit solvent model as implemented in Gaussian.²³ The default cavity parameters, static and optical dielectric constants for THF and benzene were used. The impact of explicit THF coordination to Li was investigated using a microsolvation approach. The nature of optimized stationary points was checked by analytical frequency calculations. Transition state (TS) connectivity was confirmed by following the intrinsic reaction coordinate (IRC) in both directions. Harmonic frequencies were computed to estimate Gibbs energies at 298 K under 1 atm pressure using the usual harmonic approximation.

¹H NMR shielding of optimized lithium nickelate complexes were computed at the DFT level,²⁴ using the Gauge-Independent Atomic Orbital (GIAO) method.^{25–29} For these calculations,

EPR-III basis sets³⁰ were used for H atoms to better describe the electronic density around the nuclear region.

Micro-kinetics integrations were performed using the COPASI software.³¹ Initial species concentrations were defined accordingly to the experimental conditions (see Figure S26). To simulate equilibria between intermediates, fast reactions were inferred, based on the computed equilibrium constant $K = \exp(-\Delta_r G/RT) = k_f/k_r$. Kinetic constants k_f and k_r have been chosen large enough to account for a fast reaction, and to fit with the thermodynamics of the equilibria. Natural Population Analysis (NPA) was performed with Gaussian 09 calling the NBO 6 code.³² The Electron Localized Function (ELF) and condensed DFT functions analyses were performed using the Multiwfn package.³³

Standard state correction on going from the gas phase standard state (1 atm) to the more relevant solute state (1 mol L⁻¹) was applied. This $\Delta_r G_{1\text{atm}}$ to $\Delta_r G_{1\text{M}}$ correction is of 1.89 kcal mol⁻¹ for an associative pathway ($\Delta_r \nu = -1$).³⁴

Finally, structures optimized in benzene are tagged **X**, whereas structures computed in THF are tagged **X'**. Covalent bonds are indicated with plain lines, non-covalent bonds are indicated by hashed lines and bond formed or broken during transition states are indicated by bolded hashed lines.

RESULTS AND DISCUSSION

Speciation of Lithium Nickelates in THF solution. As evidenced by ¹H NMR spectroscopy, the addition of 1 equivalent of PhLi to Ni(COD)₂ in THF leads to the formation of two lithium nickelate complexes that are in equilibrium. These species have been experimentally attributed to [Li₂(THF)₄Ph₂Ni(COD)] and [Li(THF)₂PhNi(COD)], and it has been observed that their relative proportion depends on the total concentration of the solution.¹⁵ Computationally, lithium nickelate complexes potentially formed upon successive addition of PhLi to Ni(COD)₂ (**1'**) and COD dissociations were optimized at the DFT level. Their stability was assessed relative to separated Ni(COD)₂ (**1'**) and [PhLi(THF)₂]₂ used as reference states.

As shown in **Figure 1**, COD dissociation from Ni(COD)₂ (**1'**) to form [Ni(COD)] (**2'**) is endergonic by 34.2 kcal mol⁻¹ and thus thermodynamically unfeasible. Conversely, the co-complexation of [PhLi(THF)₂]₂ with Ni(COD)₂ (**1'**) to form the mono-nickelate complex [PhLi₂(THF)₄PhNi(COD)₂] (**3'**) is computed exergonic by 1.1 kcal mol⁻¹. Dissociation of one COD from **3'** leads to the formation of the di-nickelate complex [Li₂(THF)₄Ph₂Ni(COD)] (**4'**) in which Ni⁰ is directly bonded to two Ph groups. Relative to **1'** and [PhLi(THF)₂]₂, the formation of **4'** is computed exergonic by 13.3 kcal mol⁻¹, in agreement with the experimental isolation and characterization of this complex.¹⁵ The release of one [PhLi(THF)₂] unit from **3'** to yield [Li(THF)₂PhNi(COD)₂] (**5'**) is also computed thermodynamically favorable (-2.8 kcal mol⁻¹) but to a lesser extent than the release of COD. Starting from **5'**, further dissociation of one COD to yield complex [Li(THF)₂PhNi(COD)] (**6'**) is endergonic by 14.0 kcal mol⁻¹ and is thus unlikely, although its formation was previously inferred experimentally based on estimated molecular weights determined by ¹H DOSY NMR spectroscopy.¹⁵

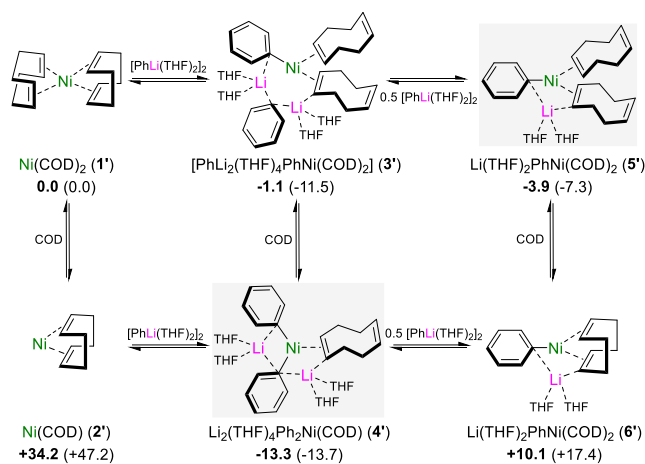


Figure 1. Structures and Gibbs energy (enthalpy) of lithium nickelates potentially formed upon addition of PhLi to Ni(COD)₂ (1') in THF. Energies are given in kcal mol⁻¹ and are relative to separated Ni(COD)₂ (1') and [PhLi(THF)₂]₂.

Based on this apparent contradiction, additional computational speciation of the structures of mono-nickelate complexes formed in THF solution combined with DFT ¹H NMR calculations and proportioning simulations were performed. As shown in **Tables S1a–d**, calculated ¹H NMR chemical shifts of [Li₂(THF)₄Ph₂Ni(COD)] (4') and [Li(THF)₂PhNi(COD)₂] (5') fit well with experimental ones. This suggests that complexes 4' and 5' are the species formed under experimental conditions. This is further supported by the simulation of the relative proportions of nickel complexes for equimolar solutions of Ni(COD)₂ and PhLi(THF)₂ at various total concentrations (**Figure S1a**).

Oxidative addition of Lithium Nickelates in THF solution.

The activity of complexes [Li₂(THF)₄Ph₂Ni(COD)] (4') and [Li(THF)₂PhNi(COD)₂] (5') towards oxidative addition of 2-methoxynaphthalene in THF solution was then computationally investigated. As shown in **Figures S2–S3**, the energy barriers are too high and thus account for the lack of reactivity observed experimentally in THF solution at ambient temperature (31.7 kcal mol⁻¹ for complex 4' and 47.7 kcal mol⁻¹ for complex 5'). It should be noted however that the competing *ortho*-lithiation of 2-methoxynaphthalene by PhLi also occurs in THF solution or when using low-aggregated PhLi dimers or monomers, even in the absence of Ni.¹⁵ Nevertheless, stoichiometric reactions between 4' and 2-methoxynaphthalene shows that the rate of the oxidative addition and cross-coupling is heavily dependent on the nature of the Li-donor ligand: slower reaction rates were observed for stronger donors.¹⁵

Speciation of Lithium Nickelates in benzene solution. The speciation of lithium nickelates was broadened to the case of “PhLi(THF)” in benzene solution (**Figure 2a**). The Gibbs energy of the resulting heterobimetallic nickelate complexes was computed relative to separated Ni(COD)₂ (1) and [PhLi(THF)₂] in benzene, in the absence of additional free THF. Compared to the speciation performed in THF solution (see **Figure 1**), in benzene and in the presence of only one THF *per* lithium center, similar nickelate complexes (3 to 5) are formed but the span of

their Gibbs energies is significantly narrowed. Co-complexation of [PhLi(THF)₂]₂ with Ni(COD)₂ to yield [PhLi₂(THF)₂PhNi(COD)₂] (3) is computed exergonic by 3.5 kcal mol⁻¹ (**Figure 2a**). In contrast with the THF solution case, the formation of [Li(THF)PhNi(COD)₂] (5) is endergonic by 4.5 kcal mol⁻¹. In benzene solution, the dissociation of COD from 3 to yield [Li₂(THF)₂Ph₂Ni(COD)] (4) is still exergonic but only by 1.2 kcal mol⁻¹, a lesser extent than in THF solution. Since the Gibbs energies of [PhLi₂(THF)₂PhNi(COD)₂] (3) and [Li₂(THF)₂Ph₂Ni(COD)] (4) are close, they both likely coexist in equilibria at ambient temperature. THF exchange from the Li centers of [PhLi(THF)₂] to those of 4 has also been considered. In this case, the formation of the di-solvated 2:1 lithium nickelate 4a is thermoneutral relative to 4 (**Figure 2a**).

Oxidative addition of Lithium Nickelates in benzene solution.

Starting from [Li₂(THF)₂Ph₂Ni(COD)] (4), and compared to the oxidative addition pathway involving [Ni(COD)] (**Figure S4**), the overall Gibbs energy barrier for the oxidative addition mediated by [Li₂(THF)₂Ph₂Ni(COD)] (4) is decreased by 11 kcal mol⁻¹ (**Figure S4**). This decrease in energy barrier is enabled by Li⁺ that promotes the binding of 2-methoxynaphthalene to the nickelate complex, and by the second “ancillary” Ph substituent that favors the displacement of COD. However, the oxidative addition energy barrier *via* this pathway remains too high to account for the reactivity observed experimentally (+35.8 kcal mol⁻¹, **Figure 2** and **TS3** in **Figure S4**). This high energy barrier most likely results from the transfer of the electronic density from the Ph groups to the COD instead of the σ*-C–O antibonding orbital. In this interaction scheme, the Ni center acts as an electron density shuttle as supported by the NBO charge analysis displayed in **Figure S5**. The lower energy barrier computed for the oxidative addition of the C_{aryl}–OMe bond to complex [Li₂(THF)₂Ph₂Ni(COD)] (4) mainly originates from a facilitated release of COD that in turn reduces the endergonicity of 2-methoxynaphthalene coordination without modifying the oxidative addition step. Based on this observation, we assessed the influence of the de-coordination of the second COD on the oxidative addition barrier.

In the absence of 2-methoxynaphthalene, the dissociation of the second COD from [Li₂(THF)₂Ph₂Ni(COD)] (4) is computed endergonic by 18 kcal mol⁻¹ (**Figure S6**). However, in the presence of 2-methoxynaphthalene, the formation of a nickelate adduct in which both COD ligands are dissociated is thermodynamically accessible. Indeed, COD dissociation starting from [NaphOMe·Li₂(THF)₂Ph₂Ni(COD)] (9) to yield [Li₂(THF)₂Ph₂Ni(η²-NaphOMe)] (13) is only endergonic by 4.8 kcal mol⁻¹ (**Figure 2a–b**). Interestingly, relative to complex 4, adduct 13 has an improved ability to perform the oxidative addition as indicated by a computed overall energy barrier of 19.5 kcal mol⁻¹, which is *ca.* 16 kcal mol⁻¹ less than for the pathway in which one COD remains bonded Ni⁰ such as in complex [Li₂(THF)₂Ph₂Ni(COD)] (4) (**Figures 2b, S4 and S7**). In the produced [Li₂(THF)₂(OMe)Ph₂Ni(Naph)] (14), the methoxy group is bonded to the Li centers, and not interacting with Ni, so that the reaction can be viewed as a σ-bond metathesis rather than an oxidative addition.^{35,36}

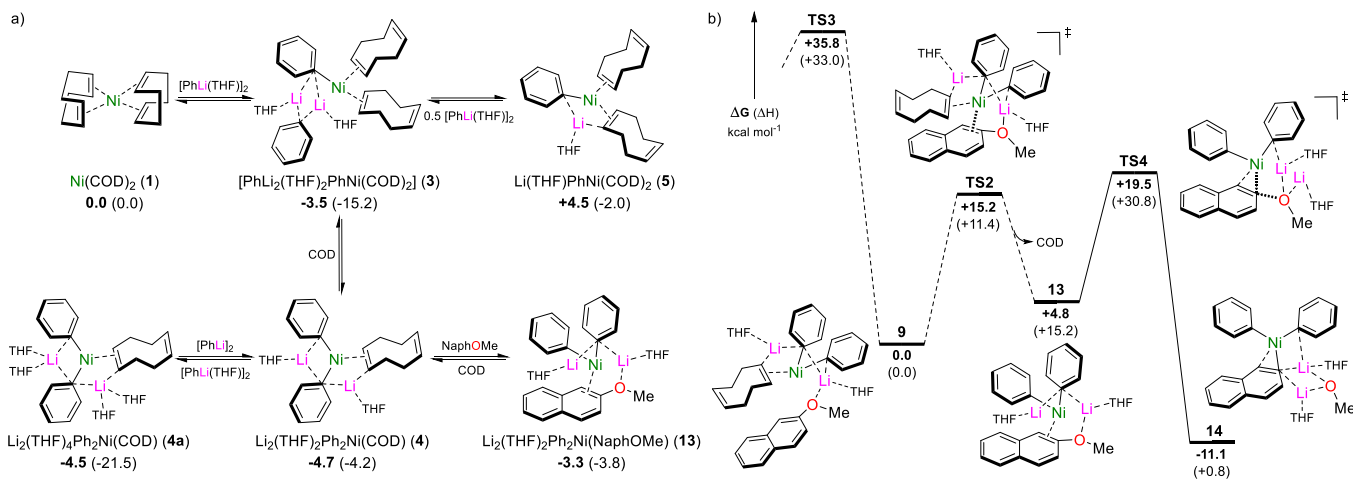


Figure 2. a) Structures and Gibbs energy (enthalpy) of the lithium nickelate complexes potentially formed under addition of PhLi(THF) to Ni(COD)₂ (1) in benzene. Energies are given with respect to Ni(COD)₂ (1) and [PhLi(THF)]₂. The coordination of 2-methoxynaphthalene (NaphOMe) to complex (4) is favored and prompts the release of the second COD to form [Li₂(THF)₂Ph₂Ni(NaphOMe)] (13). b) Reaction pathway for the second COD release (TS2) and subsequent oxidative addition (TS4) in benzene. Energies are given in kcal mol⁻¹ (see Figure S4 for alternative pathways).

In terms of electronic properties, the activation of the C_{aryl}-OMe bond by Ni⁰ is facilitated by the increased donation ability of the [Li₂Ph₂Ni⁰]-ate-moiety to 2-methoxynaphthalene as indicated by the augmentation of the negative NPA charge of the 2-methoxynaphthalene group upon COD release [(-0.87 |e⁻| vs. 0.03 |e⁻|), see **Figure S8**]. This effect is also visible in the geometry of TS4. The C_{aryl}-OMe bond length increases from 1.78 Å to 1.84 Å relative to TS3 (**Figure 2b**). Once again, as in the case of [Li₂(THF)₂Ph₂Ni(COD)] (4, see above), Ni is acting as an electron density shuttle between the Ph groups and the naphthalene moiety with little charge variation on the Ni itself (**Figure S5**).

To summarize this section, the rate determining step of the cross-coupling reaction is the oxidative addition of 2-methoxynaphthalene to the ate-complex [Li₂(THF)₂Ph₂Ni(COD)] (4) via the di-nickelate complex [Li₂(THF)₂Ph₂Ni(η²-NaphOMe)] (13). Coordination of PhLi(THF) and 2-methoxynaphthalene to Ni⁰ promotes the consecutive dissociation of two COD ligands. PhLi(THF) facilitates oxidative addition by improving the electron donating ability of Ni⁰ whilst Li acts as a Lewis acid to coordinate and prime the oxidative addition of the C_{aryl}-OMe bond of 2-methoxynaphthalene. This demonstrates that Ni and Li truly work cooperatively to enable this challenging catalytic transformation under mild reaction conditions.

Possible Involvement of LiOMe. Our previously reported monitoring of the cross-coupling reaction between 2-methoxynaphthalene and PhLi catalyzed by Ni(COD)₂ in benzene shows three apparent stages with different reaction rates (**Figure S9**).¹⁵ The first one can be seen as an induction period, the second one is the fastest, and the third one indicates a possible deactivation of the system. To account for this phenomenon, the influence of a potential Li-based by-product [PhLi-LiOMe(THF)₂]₂, which results from the aggregation of MeOLi and PhLi, on the reactivity was assessed computationally.

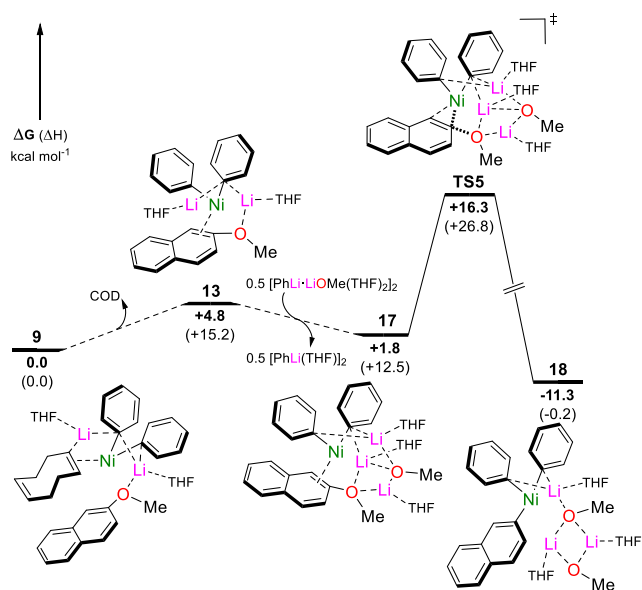


Figure 3. Structures and Gibbs energy (enthalpy) of the reaction pathway for the oxidative addition of 2-methoxynaphthalene to lithium nickelates under the co-existence of [PhLi-LiOMe(THF)₂]₂ and [PhLi(THF)₂] in benzene. The most stable adduct 9 was used as an energy reference. Energies are given in kcal mol⁻¹.

In the presence of [PhLi-LiOMe(THF)₂]₂ release of COD and binding of 2-methoxynaphthalene to yield complex 17 is almost thermoneutral (**Figure 3**, see **Figure S10** for possible intermediates). From 17, the oxidative addition step requires to overcome a Gibbs energy barrier of 14.5 kcal mol⁻¹ to proceed (**Figure 3**). This barrier is almost equal to the one previously commented in the absence of LiOMe (14.7 kcal mol⁻¹, **Figures 2b** and **S7**). NBO charge analysis reveals that, in the absence or presence of LiOMe, the 2-methoxynaphthalene adduct and transition state of oxidative addition share very similar charge distribution as illustrated in **Figure S11**.

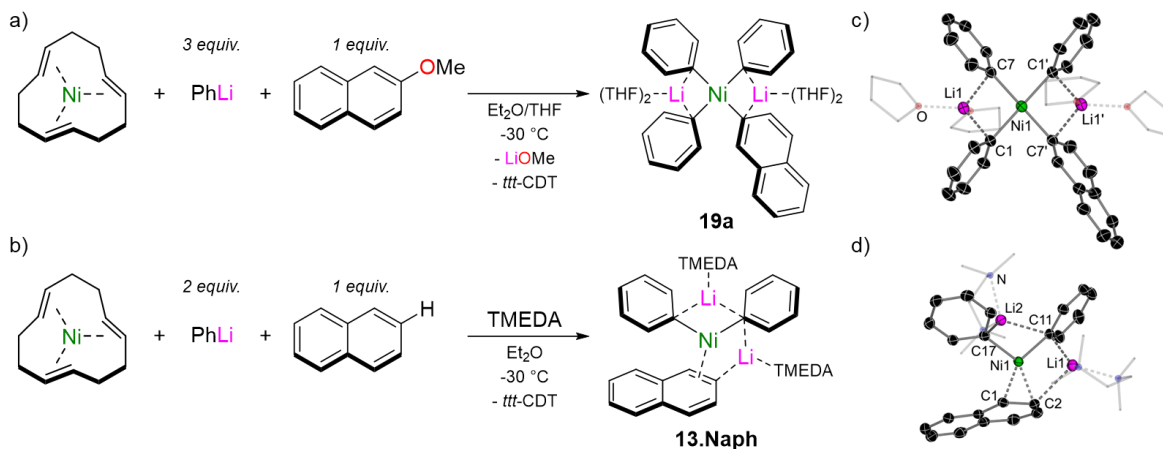


Figure 4. a) Synthesis of heteroleptic oxidative addition product $\text{Li}_2(\text{THF})_4\text{Ph}_3\text{Ni}(\text{Naph})$ (**19a**). b) Synthesis of coordination complex $\text{Li}_2(\text{TMEDA})_2\text{Ph}_2\text{Ni}(\eta^2\text{-naphthalene})$ (**13.Naph**). c) Molecular structure of $\text{Li}_2(\text{THF})_4\text{Ph}_3\text{Ni}(\text{Naph})$ (**19a**). Hydrogen atoms omitted and coordinated THF shown as wireframe for clarity. d) Molecular structure of $\text{Li}_2(\text{TMEDA})_2\text{Ph}_2\text{Ni}(\eta^2\text{-naphthalene})$ (**13.Naph**). Hydrogen atoms omitted and coordinated TMEDA shown as wireframe for clarity.

Relative to the most stable dormant complex **9** and in the presence of LiOMe, oxidative addition of 2-methoxynaphthalene proceeds *via* **TS5** (Figure 3) with an overall Gibbs energy barrier of $16.3 \text{ kcal mol}^{-1}$, *i.e.* $3.2 \text{ kcal mol}^{-1}$ less than the one computed in absence of LiOMe *via* **TS4** (Figure 2b). This reactivity trend jointly results from an easier coordination of 2-methoxynaphthalene and an easier decoordination of COD in presence of lithium methoxide. The enhanced catalytic activity that is characteristic of the second stage of the kinetic profile is therefore proposed to result from the non-innocent behavior of LiOMe that is concomitantly produced by the reaction. Finally, the reaction slowing down could be due to PhLi deactivation during the reaction. For instance, due to the co-precipitation of PhLi with MeOLi in stable adducts such as $[\text{PhLi}_2\text{OMe}(\text{THF})_2]$. Experimentally however, attempts to confirm or rule out the involvement of LiOMe or mixed aggregates were inconclusive, likely due to the insolubility of LiOMe in THF or benzene (see SI for full details).

Isolation of Identified Intermediates. With several potential intermediates identified by the computational studies, we next set out to experimentally validate some of these species. We have previously demonstrated that the treatment of *in situ* generated $\text{Li}_2(\text{solvent})_4\text{Ph}_2\text{Ni}(\text{COD})$ (**4**) with 2-methoxynaphthalene leads to cross-coupling and clean regeneration of $\text{Ni}(\text{COD})_2$ (**1**).¹⁵ Whilst the rate of the coupling reaction was found to depend on the identity of the donor or solvent, which supports the initial coordination of the substrate to Li^+ , no intermediates could be isolated or spectroscopically observed. We therefore turned to $\text{Ni}(\text{ttd-CDT})$ (where CDT = 1,5,9-cyclododecatriene) as an alternative Ni^0 source, since the *ttd-CDT* olefin is known to be more labile when compared to COD.^{37,38}

Treatment of $\text{Ni}(\text{ttd-CDT})$ with 3 equivalents of PhLi and 1 equivalent of 2-methoxynaphthalene at $-30 \text{ }^\circ\text{C}$ afforded yellow crystals, which were identified as the oxidative addition product $[\text{Li}_2(\text{THF})_4\text{Ph}_3\text{Ni}(\text{Naph})]$ (**19a**) by single-crystal X-ray diffraction (Figure 4a). This compound forms regardless of PhLi stoichiometry, indicating that its formation is favorable over a lower order (*i.e.* 1:1 Li/Ni^{II} ratio) species. Since the C–OMe bond cleavage and oxidative addition occurs readily even at low temperatures, we turned to naphthalene as an inert substitute to seek the η^2 -coordination proposed in intermediate **13**. Gratifyingly, treatment of $\text{Ni}(\text{ttd-CDT})$ with 2 equivalents of PhLi and

1 equivalent of naphthalene at $-30 \text{ }^\circ\text{C}$ in the presence of TMEDA (where TMEDA = *N,N,N',N'*-tetramethylethylenediamine) afforded deep red crystals of the target complex $\text{Li}_2(\text{TMEDA})_2\text{Ph}_2\text{Ni}(\eta^2\text{-naphthalene})$ (**13.Naph**, Figure 4b).

In compound **19a**, the Ni^{II} center adopts a square planar geometry (Figure 4c) and shows similar structural features to the homoleptic analogue, $\text{Li}_2(\text{THF})_4\text{Ph}_4\text{Ni}$.³⁹ In compound **13.Naph**, the Ni^0 center adopts a pseudo-trigonal planar confirmation (Figure 4d) and shows similar structural features to the previously characterized $\text{Li}_2(\text{solvent})_n\text{Ph}_2\text{Ni}(\text{COD})$ complexes.¹⁵ A comparison of the structural and spectroscopic features of **13.Naph** with $\{\text{Cy}_2\text{PC}_3\text{H}_6\text{PCy}_2\}\text{Ni}(\eta^2\text{-naphthalene})$ ⁴⁰ illustrate the high σ -donating ability of the phenyl-carbanion ligands when compared to typically employed neutral phosphine or *N*-heterocyclic carbene ligands. For example, in the ¹H NMR spectrum, $\{\text{Cy}_2\text{PC}_3\text{H}_6\text{PCy}_2\}\text{Ni}(\eta^2\text{-naphthalene})$ displays a broad singlet at $\delta 5.75$ for the coordinated naphthalene ring,⁴⁰ whilst compound **13.Naph** displays two well-resolved multiplets at $\delta 4.96$ and $\delta 4.26$ (in C_6D_6) or $\delta 4.24$ and $\delta 4.09$ (in THF-d_8). Similarly, the C1=C2 distance in $\{\text{Cy}_2\text{PC}_3\text{H}_6\text{PCy}_2\}\text{Ni}(\eta^2\text{-naphthalene})$ is $1.435(3) \text{ \AA}$,⁴⁰ and $1.462(2) \text{ \AA}$ in **13.Naph**. These features are indicative of significant backdonation from the electron-rich Ni^0 center into the C=C π^* orbital which is elongated by 0.09 \AA relative to free naphthalene [$1.373(1) \text{ \AA}$].⁴¹

Reductive Elimination from Nickel(II) Intermediates. Computationally, the exchange of LiOMe with PhLi to afford compound $\text{Li}_2(\text{THF})_2\text{Ph}_3\text{Ni}(\text{Naph})$ (**19**) is exergonic by $32.8 \text{ kcal mol}^{-1}$ (Figure 5), in agreement with experimental studies. Remarkably, reductive elimination from **19** or **26** (with co-complexed LiOMe) are selective towards the formation of the cross-coupled product over the homo-coupled species (Figures 5, S14 and S16). The formation of homo-coupling products *via* reductive elimination from complex **19** to yield complex **25** raises the question of the catalyst regeneration. Indeed, complex **25** can undergo 2-methoxynaphthalene/COD exchange, subsequent oxidative addition, and reductive eliminations to yield 2-phenylnaphthalene, biphenyl and 2,2'-binaphthyl with low selectivities (**TS16** to **TS18** in Figures S18–S20) as summarized in Figure S21. Interestingly, these pathways lead to the formation of complex $[\text{NaphOMe}\cdot\text{Li}_2(\text{THF})_2(\text{Naph})_2\text{Ni}(\text{COD})]$ (**48**) that only differs from complexes $[\text{NaphOMe}\cdot\text{Li}_2(\text{THF})_2\text{Ph}_2\text{Ni}(\text{COD})]$ (**9**) and

[NaphOMe·Li₂(THF)₂(Ph)(Naph)Ni(COD)] (**25**) by the relative proportion of Ph and Naph groups bonded to Ni. The reactivity and selectivities of **48** relative to the oxidative addition of 2-NaphOMe and subsequent reductive eliminations have also been investigated computationally. The energy profiles computed are very similar to those computed for complexes **9** and **25** (Figures S22–S25) and reveals that these three analogs contribute to the overall activity and the formation of both hetero- and homo-coupling products that are respectively identified in 58%, 15% and 15% yield.¹⁵

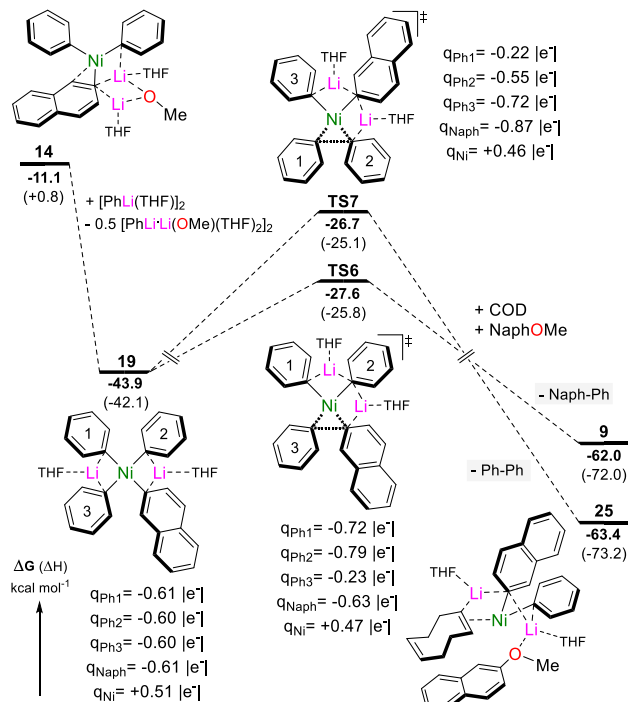


Figure 5. Structures and Gibbs energy (enthalpy) comparing the different pathways for reductive elimination and explaining the origin of selectivity between cross-coupling and homo-coupling products. Energies are given in kcal mol⁻¹.

Experimentally, the reductive elimination from Li₂(THF)₄Ph₃Ni(Naph) (**19a**) can be followed by ¹H NMR spectroscopy and occurs readily in the presence of COD (2 equivalents) to give Li₂(THF)₄Ph₂Ni(COD) (**4'**) with selective formation of 2-phenylnaphthalene [71% GC yield; biphenyl (9%); 2,2'-binaphthyl (2%); naphthalene (5%); **Figure 6**].

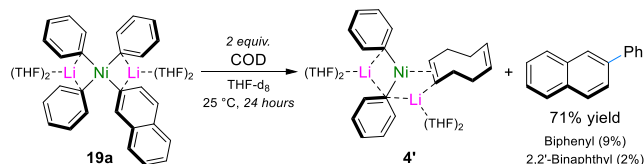


Figure 6. Reductive elimination from Li₂(THF)₄Ph₃Ni(Naph) (**19a**) in the presence of COD to give Li₂(THF)₄Ph₂Ni(COD) (**4'**), 2-phenylnaphthalene, biphenyl and 2,2'-binaphthyl.

To complement, as we have shown experimentally that the selectivity of the reaction depends on the availability of

[PhLi(THF)]₂, we have also investigated the reactivity of complex [Li₂(THF)₂Ph₂Ni(Naph)(OMe)] (**14**) that is the resting state of the catalyst when the concentration of [PhLi(THF)]₂ is low. In this case, the lowest energy profile leads to the formation of biphenyl *via* **TS11** over the formation of the cross-coupling product (**Figure S17**).

To summarize this mechanistic section, three complexes that can be formulated as [NaphOMe·Li₂(THF)₂(R)(R')Ni(COD)] where R, R' = Ph, Naph] all contribute to the catalytic activity with slightly different selectivities between homo- and cross-coupling products. The role played by [Li₂(THF)₂Ph₂Ni(Naph)(OMe)] in modifying the selectivity of the reaction depending on the concentration of PhLi, especially at the end the reaction, has also been highlighted.

Revised Catalytic Cycle(s). The set of energy profiles computed for the Ni-catalyzed cross-coupling under study suggests an interesting mechanistic scenario that differs from previously reported pathways^{5,12,13} and that is summarized in **Figures 7a** and **S15**. It involves six key steps: (i) *Nickelate formation* (**1** → **4**) through the complexation of two “ancillary” Ph groups to promote the release of one COD from Ni(COD)₂ and to enhance the electron donating ability of Ni⁰; (ii) *Li binding* (**4** → **9**) of 2-methoxynaphthalene due to its Lewis acidic character which is key to facilitate the next step; (iii) *π-arene coordination to Ni* (**9** → **13**) that favors the release of the second COD and enables the transfer of charge density from [Li₂Ph₂Ni] moiety to the naphthyl substrate; (iv) *Rate determining oxidative addition of the C–OMe bond* (**13** → **14**) with transfer of the methoxy group to Li; (v) *LiOMe–PhLi exchange* (**14** → **19**) experimentally supported by the isolation of **19a**; (vi) *Reductive eliminations* (**19** → **4**) to selectively yield the cross-coupling product 2-phenylnaphthalene and to regenerate Ni⁰-ate complex **4**. To confidently support this overall mechanistic picture, we have solved the set of kinetic equations – by means of a microkinetic model – considering the initial experimental concentrations to simulate catalytic activity curves over time.

As mentioned above, the three nickelate complexes that feature all combinations of Ph and Naph groups are contributing to the overall selectivity and activity of the reaction and were thus included in kinetics simulations. Overall, a remarkable agreement between experimental and simulated kinetic results is obtained.¹⁵ When only cycle (a) “without involvement of LiOMe” (**Figures S15, S22, S25, S26**) was considered, the apparent zeroth order with respect with PhLi was successfully reproduced (**Figure S27a**) but the conversion of the substrate was limited relative to the experimental one.

Adjunction to cycle (a) of cycle (b) “with the joint involvement of [PhLi·LiOMe(THF)₂]₂ and PhLi” allowed to finely represent, in addition, the short induction period and the subsequent acceleration of the rate of the reaction but though increased, the final simulated conversion remained low relative to the experimental one (**Figure S27b**). Finally, the combination of cycles (a), (b) and (c) “with involvement

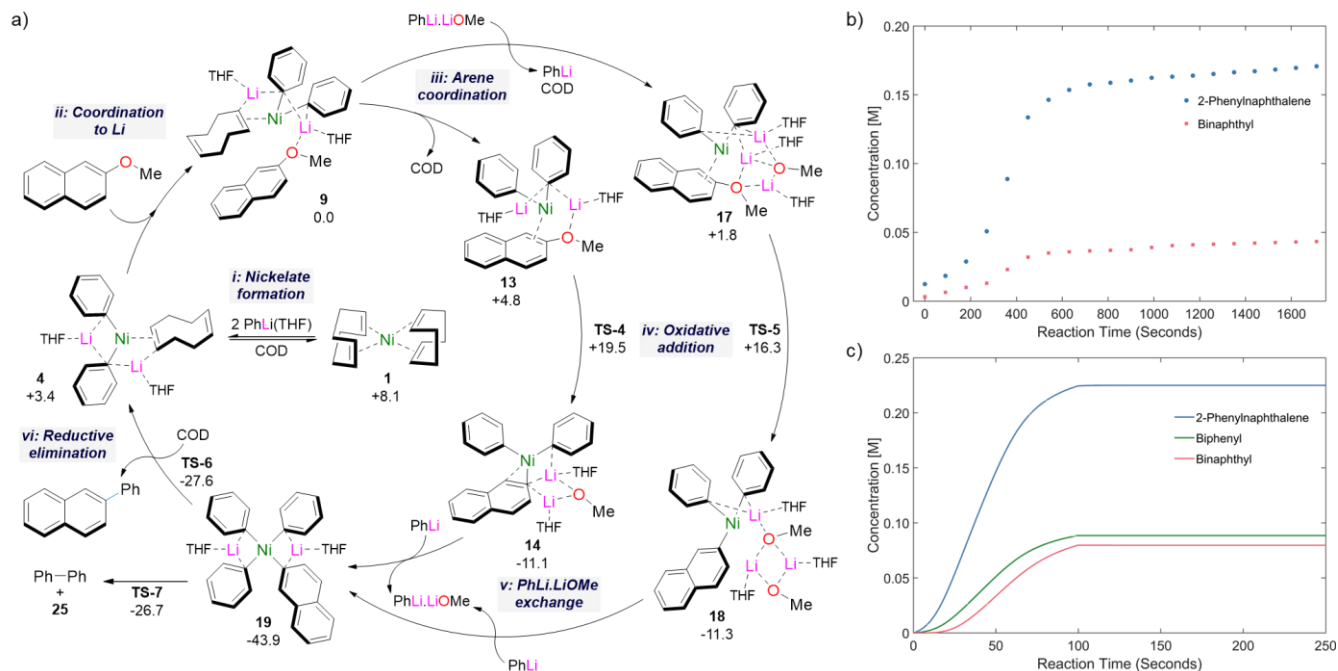


Figure 7. a) Mechanistic proposal (Structures, Gibbs energy) for the cross-coupling reaction between 2-methoxynaphthalene (0.4 M) and phenyl-lithium (0.44 M) catalyzed by Ni(COD)₂ (5 mol%) (**1**) in benzene. Energies [±] are given in kcal mol⁻¹ with respect to [NaphOMe·Li₂(THF)₂Ph₂Ni(COD)] (**9**), [PhLi(THF)]₂ and [PhLi₂(OMe)(THF)₂]. (+/-) is the regenerative energy of complex **1**, **4** and **9**. The complexes are named with black bold numbers. b) A plot of concentration (M) vs. time (seconds) for the cross-coupled product 2-phenylnaphthalene and homo-coupled 2,2'-binaphthyl by experimental work. c) Micro-kinetics integration obtained by stationary state simulation (see also **Figures S15, S22** and **S26**).

of [PhLi·LiOMe(THF)₂]₂ only” (**Figures 7c** and **S27**) afforded an almost ideal simulation of the experimental kinetic profile (**Figure 7b**).

Unlocking the “Naphthalene Problem”. With this mechanistic knowledge in hand, we next sought to use these insights to try and overcome a current challenge in Ni-catalysis, the so-called “naphthalene problem”.⁵ This phenomenon generally restricts the electrophilic coupling partner to π-extended systems, such as 2-methoxynaphthalene, meaning that C–C cross-couplings of unbiased aryl ethers such as anisole itself is rare.^{8–10}

Computationally, the oxidative addition of anisole to Ni⁰-ate complex **4** accordingly to a mechanism analogous to the one computed for 2-methoxynaphthalene in the presence of [PhLi(THF)]₂ in benzene was assessed. In this case, a Gibbs energy barrier of 26.4 kcal mol⁻¹ was computed for the C_{aryl}–OMe oxidative addition (**Figure S28**). This trend agrees with the expected lower reactivity of non π-extended derivatives compared to the naphthyl-derived system, but this value remains too high to account for a feasible transformation at room temperature.

In the absence of any coordinating THF however, the addition of one more equivalent of [PhLi]₂ to complex **1** to yield the higher-order lithium nickelate complex [Li₄Ph₄Ni(COD)] (**62**) is exergonic by 19.8 kcal mol⁻¹ (**Figures 8** and **S29**). Notably, we have previously demonstrated that the further co-complexation of additional molecules of organolithium (which are not directly coordinated to Ni⁰) has been shown to be possible for several lithium nickelates, particularly in weakly coordinated solvent systems.^{15,42–45} From complex **62**, oxidative addition of anisole proceeds after COD release with an overall Gibbs energy barrier of 16.5 kcal mol⁻¹ (**Figures 8** and **S31**). This

suggests that anisole activation can occur under THF-free conditions.

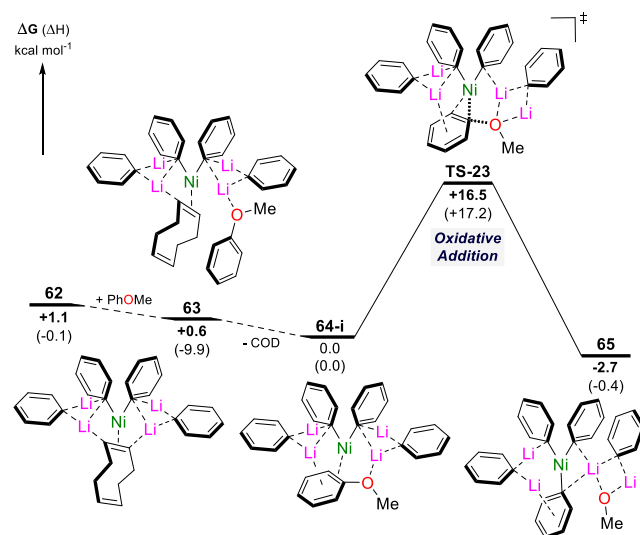


Figure 8. Structures and Gibbs energy (enthalpy) for the oxidative addition of anisole to lithium nickelates formed from Ni(COD)₂ and [PhLi]₂ in benzene. The most stable adduct **64-i** was used as an energy reference. Energies are given kcal mol⁻¹.

Experimentally, the cross-coupling reaction between anisole and PhLi catalyzed by Ni(COD)₂ was enabled simply by using the aryl ether substrate in a sufficient excess in pure benzene (**Figure 9a**). This has two consequences: (i) it enables the solubilization of PhLi and any lithium nickelate intermediates; and (ii) promotes the dissociation of COD

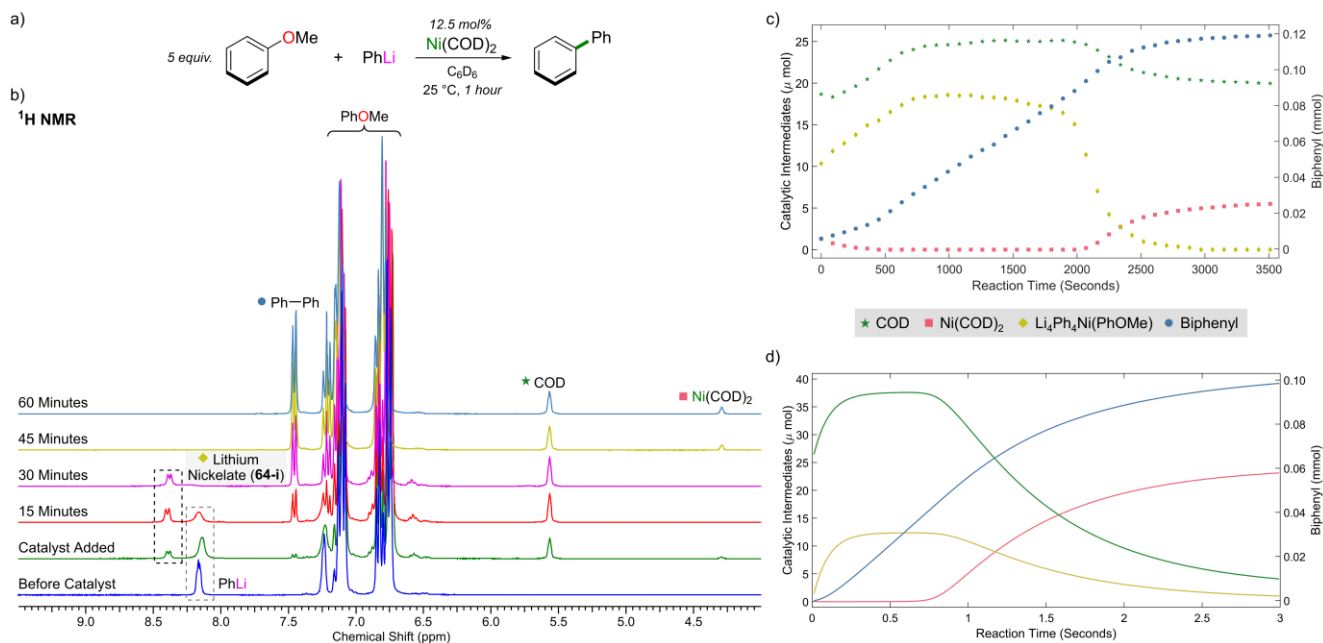


Figure 9. a) Ni(COD)₂ catalyzed cross-coupling of anisole with PhLi. c) Experimental reaction profile showing the quantities of biphenyl, Ni(COD)₂, COD, and the proposed lithium nickelate intermediate [Li₄Ph₄Ni(PhOMe)] (**64-i**) over time. d) Simulated reaction profile over time based on the steady state approximation (see **Figure S34**, and *pathway i* of **Figure S36**).

through η^2 -arene coordination of anisole, as identified computationally and confirmed experimentally. The solubility of PhLi and the rate of the cross-coupling reaction was monitored with 0.5 to 8 equivalents of anisole. Complete solubility of PhLi requires 7 to 8 equivalents of anisole (**Figure S45**), whilst the optimal cross-coupling rates are observed with 2 to 3 equivalents of anisole (**Figure S47**). Regardless of the experimental conditions however (equivalents of PhOMe, catalyst loading, reaction time), the yield of biphenyl never exceeded ~60% with respect to PhLi. This may be attributed to co-precipitation of PhLi with the LiOMe by-product, or due to the observation that multiple equivalents of PhLi co-complex per Ni center to form the active lithium nickelate intermediates (see **Figure 8**).

The ¹H NMR spectra of the reaction with 1 equivalent of PhLi, 5 equivalents of PhOMe and 12.5 mol% of Ni(COD)₂ is shown in **Figure 9b**. Upon addition of Ni(COD)₂, a new doublet signal ($J = 7.0$ Hz) appears at δ 8.4 ppm which is attributed to the formation of an anisole-solvated lithium nickelate complex. The Gibbs energies of [Ph₄Li₄PhNi(COD)] (**62**), [Ph₄Li₄PhNi(COD)(PhOMe)] (**63**) and [Ph₄Li₄PhNi(PhOMe)] (**64-i**) are all similar (see also **Figure S29** for additional structures), suggesting that they likely coexist in solution at ambient temperature. The calculated ¹H NMR spectrum of complex **64-i** however was found to match well with the detected signals (**Table S2**). Spectroscopic monitoring of the reaction over 60 minutes shows the clean formation of biphenyl (60% yield after 1 hour) with concomitant consumption of PhLi and the proposed lithium nickelate intermediate (**64-i**), along with the partial regeneration of Ni(COD)₂ (**Figures 9b-c**).

Experimental kinetic studies indicate that the reaction is first-order in catalyst concentration (**Figure S48-50**), as previously observed for the 2-methoxynaphthalene/PhLi/Ni(COD)₂ catalytic system.¹⁵ An apparent zeroth-order with respect to PhLi and PhOMe is observed consistent with the fast formation of detected intermediate (**64-i**) and the subsequent rate determining oxidative addition (**Figure S39**). Worthy of note, the addition of another equivalent of PhLi to the reaction mixture after

45 minutes appears to restart the reaction (**Figures S38 and S51**), illustrating the stability of the Ni-catalyst and potential deactivation of PhLi under the reaction conditions, which are likely due to solubility issues or co-complexation with the LiOMe by-product.

Further validation of this mechanistic proposal using kinetic modelling with COPASI³¹ successfully reproduces the apparent zeroth-order dependance with respect to PhLi and PhOMe, intermediate concentration patterns and PhLi spiking tests (**Figure S38-40**). However, simulated reaction times are shorter than those determined experimentally (**Figures 9c-d**). This suggests that the overall Gibbs energy barrier for oxidative addition can be slightly underestimated but additional solubility/physico-chemical issues – that are not modelled – can also contribute to the time scale description in kinetic profiles.

CONCLUSIONS

By combining detailed theoretical calculations with spectroscopic and kinetic investigations, together with the isolation of key organometallic intermediates, new mechanistic insights have been provided in the Ni-catalyzed cross-coupling reaction of phenyl-lithium and aromatic ethers using Ni(COD)₂. Underpinned by bimetallic cooperativity, these reactions involve the formation of highly reactive lithium nickelates. A six-step reaction mechanism is proposed in which each metal plays a pivotal role. Using 2-methoxynaphthalene as a model substrate; initially two equivalents of PhLi undergo co-complexation with Ni(COD)₂ to form an electron rich lithium nickelate [Li₂(THF)₂Ph₂Ni(COD)] (**4**) with the release of one equivalent of COD (*step 1*) to which the aromatic ether can coordinate *via* Li...O interaction (*step 2*) which facilitates the displacement of the remaining COD ligand through π -coordination of the naphthyl ring to Ni (*step 3*). This coordination enables the efficient charge transfer from the nickelate to the substrate which is required to promote the oxidative cleavage of the C_{aryl}-OMe bond which is the rate determining step, with concomitant formation of LiOMe (*step 4*). Exchange of co-complexed LiOMe with

PhLi (*step 5*), followed by reductive elimination (*step 6*) furnishes the cross-coupled product 2-phenylnaphthalene and regenerates the lithium Ni⁰-ate complex.

This mechanistic proposal not only provides a rationale for the dramatic solvent effects previously noted for this reaction but also uncovers the multiple roles of lithium in facilitating this Ni-catalyzed process. Furthermore, building on this knowledge, the well-known “naphthalene problem” for these reactions can be addressed, as demonstrated when using anisole as a cross-coupling partner.

ASSOCIATED CONTENT

Supporting Information

The Supporting Information is available free of charge on the ACS Publications website. Additional energy profiles, electron density analyses, experimental procedures, and spectral data are provided (pdf). Cartesian coordinates of all the optimized structures and their associated uncorrected (XYZ) and corrected (pdf) energies are provided.

AUTHOR INFORMATION

Corresponding Authors

* Eva Hevia. E-mail: e.hevia@unibe.ch

* Marie-Eve L. Perrin. E-mail: marie-eve.perrin@univ-lyon1.fr

* Pierre-Adrien Payard. E-mail: pierre-adrien.payard@univ-lyon1.fr

Author Contributions

‡ HL and AMB contributed equally to this work. Experiments were performed by AMB, computations were performed by HL. EH, PAP and MEP supervised the overall project. The manuscript was written through contributions of all authors.

ACKNOWLEDGMENT

EH and AMB thank the Swiss National Science Foundation (SNF) (Project 200021_188573) and Universität Bern for their generous sponsorship of this research. H. L. thanks the Chinese Scholarship Council (CSC NO. 202009370047) for a fellowship. The authors are grateful to the CNRS, ICBMS (UMR 5246), Université Lyon 1 and the Region Auvergne Rhone Alpes for financial support. The CCIR of ICBMS, PSMN and GENCI (allocation A10, A0100812501) are acknowledged for a generous allocation of computational resources and providing technical support.

ABBREVIATIONS

CDT (1,5,9-cyclododecatriene); COD (1,5-cyclooctadiene); DFT (density functional theory); DOSY (diffusion ordered spectroscopy); NBO (natural bond orbital); NMR (nuclear magnetic resonance); TMEDA (*N,N,N',N'*-tetramethylethylenediamine); THF (tetrahydrofuran).

REFERENCES

- (1) Zarate, C.; van Gemmeren, M.; Somerville, R. J.; Martin, R. Phenol Derivatives: Modern Electrophiles in Cross-Coupling Reactions. In *Advances in Organometallic Chemistry*; Elsevier Inc., 2016; Vol. 66, pp 143–222. <https://doi.org/10.1016/bs.adomc.2016.07.001>.
- (2) Rosen, B. M.; Quasdorf, K. W.; Wilson, D. A.; Zhang, N.; Resmerita, A.; Garg, N. K.; Percec, V. Nickel-Catalyzed Cross-Couplings Involving Carbon–Oxygen Bonds. *Chem. Rev.* **2011**, *111* (3), 1346–1416. <https://doi.org/10.1021/cr100259t>.
- (3) Qiu, Z.; Li, C. J. Transformations of Less-Activated Phenols and Phenol Derivatives via C–O Cleavage. *Chem. Rev.* **2020**, *120* (18), 10454–10515.

- (4) Tobisu, M.; Chatani, N. Cross-Couplings Using Aryl Ethers via C–O Bond Activation Enabled by Nickel Catalysts. *Acc. Chem. Res.* **2015**, *48*, 1717–1726. <https://doi.org/10.1021/acs.chemrev.0c00088>.
- (5) Borys, A. M.; Hevia, E. Mechanisms of the Nickel-Catalyzed Hydrogenolysis and Cross-Coupling of Aryl Ethers. *Synthesis* **2022**, *54* (13), 2976–2990. <https://doi.org/10.1055/a-1806-4513>.
- (6) Wenkert, E.; Michelotti, E. L.; Swindell, C. S. Nickel-Induced Conversion of Carbon–Oxygen into Carbon–Carbon Bonds. One-Step Transformations of Enol Ethers into Olefins and Aryl Ethers into Biaryls. *J. Am. Chem. Soc.* **1979**, *101* (8), 2246–2247. <https://doi.org/10.1021/ja00502a074>.
- (7) Zarate, C.; Nakajima, M.; Martin, R. A Mild and Ligand-Free Ni-Catalyzed Silylation via C–OMe Cleavage. *J. Am. Chem. Soc.* **2017**, *139*, 1191–1197. <https://doi.org/10.1021/jacs.6b10998>.
- (8) Dankwardt, J. W. Nickel-Catalyzed Cross-Coupling of Aryl Grignard Reagents with Aromatic Alkyl Ethers: An Efficient Synthesis of Unsymmetrical Biaryls. *Angew. Chem. Int. Ed.* **2004**, *43* (18), 2428–2432. <https://doi.org/10.1002/anie.200453765>.
- (9) Xie, L. G.; Wang, Z. X. Cross-Coupling of Aryl/Alkenyl Ethers with Aryl Grignard Reagents through Nickel-Catalyzed C–O Activation. *Chem. Eur. J.* **2011**, *17* (18), 4972–4975. <https://doi.org/10.1002/chem.201003731>.
- (10) Iglesias, M. J.; Prieto, A.; Nicasio, M. C. Kumada-Tamao-Corriu Coupling of Heteroaromatic Chlorides and Aryl Ethers Catalyzed by (IPr)Ni(Allyl)Cl. *Org. Lett.* **2012**, *14* (17), 4318–4321. <https://doi.org/10.1021/ol302112q>.
- (11) Dicciani, J. B.; Diao, T. Mechanisms of Nickel-Catalyzed Cross-Coupling Reactions. *Trends Chem.* **2019**, *1* (9), 830–844. <https://doi.org/10.1016/j.trechm.2019.08.004>.
- (12) Ogawa, H.; Minami, H.; Ozaki, T.; Komagawa, S.; Wang, C.; Uchiyama, M. How and Why Does Ni⁰ Promote Smooth Etheric C–O Bond Cleavage and C–C Bond Formation? A Theoretical Study. *Chem. Eur. J.* **2015**, *21*, 13904–13908. <https://doi.org/10.1002/chem.201502114>.
- (13) Kojima, K.; Yang, Z. K.; Wang, C.; Uchiyama, M. Ethereal C–O Bond Cleavage Mediated by Ni(0)-Ate Complex: A DFT Study. *Chem. Pharm. Bull.* **2017**, *65* (9), 862–868. <https://doi.org/10.1248/cpb.c17-00487>.
- (14) Rawat, V. K.; Higashida, K.; Sawamura, M. Nickel-Catalyzed Homo-Coupling of Aryl Ethers with Magnesium Anthracene Reductant. *Synthesis* **2021**, *3*. <https://doi.org/10.1055/a-1509-5954>.
- (15) Borys, A. M.; Hevia, E. The Anionic Pathway in the Nickel-Catalyzed Cross-Coupling of Aryl Ethers. *Angew. Chem. Int. Ed.* **2021**, *60* (46), 24659–24667. <https://doi.org/10.1002/anie.202110785>.
- (16) Frisch, M. J.; Trucks, G. W.; Schlegel, H. B.; Scuseria, G. E.; Robb, M. A.; Cheeseman, J. R.; Scalmani, G.; Barone, V.; Petersson, G. A.; Nakatsuji, H.; Li, X.; Caricato, M.; Marenich, A. V.; Bloino, J.; Janesko, B. G.; Gomperts, R.; Mennucci, B.; Hratchian, H. P.; Ortiz, J. V.; Izmaylov, A. F.; Sonnenberg, J. L.; Williams-Young, D.; Ding, F.; Lipparini, F.; Egidi, F.; Goings, J.; Peng, B.; Petrone, A.; Henderson, T.; Ranasinghe, D.; Zakrzewski, V. G.; Gao, J.; Rega, N.; Zheng, G.; Liang, W.; Hada, M.; Ehara, M.; Toyota, K.; Fukuda, R.; Hasegawa, J.; Ishida, M.; Nakajima, T.; Honda, Y.; Kitao, O.; Nakai, H.; Vreven, T.; Throssell, K.; Montgomery Jr., J. A.; Peralta, J. E.; Ogliaro, F.; Bearpark, M. J.; Heyd, J. J.; Brothers, E. N.; Kudin, K. N.; Staroverov, V. N.; Keith, T. A.; Kobayashi, R.; Normand, J.; Raghavachari, K.; Rendell, A. P.; Burant, J. C.; Iyengar, S. S.; Tomasi, J.; Cossi, M.; Millam, J. M.; Klene, M.; Adamo, C.; Cammi, R.; Ochterski, J. W.; Martin, R. L.; Morokuma, K.; Farkas, O.; Foresman, J. B.; Fox, D. J. *Gaussian 09, Revision D.01*; Gaussian, Inc., Wallingford CT, 2016.
- (17) Zhao, Y.; Truhlar, D. G. The M06 Suite of Density Functionals for Main Group Thermochemistry, Thermochemical Kinetics, Noncovalent Interactions, Excited States, and Transition Elements: Two New Functionals and Systematic Testing of Four M06-Class Functionals and 12 Other Function. *Theor. Chem. Acc.* **2008**, *120* (1–3), 215–241. <https://doi.org/10.1007/s00214-007-0310-x>.
- (18) Sperger, T.; Sanhueza, I. A.; Kalvet, I.; Schoenebeck, F.

- Computational Studies of Synthetically Relevant Homogenous Organometallic Catalysis Involving Ni, Pd, Ir, and Rh: An Overview of Commonly Employed DFT Methods and Mechanistic Insights. *Chem. Rev.* **2015**, *115* (17), 9532–9586. <https://doi.org/10.1021/acs.chemrev.5b00163>.
- (19) Weigend, F. Accurate Coulomb-Fitting Basis Sets for H to Rn. *Phys. Chem. Chem. Phys.* **2006**, *8* (9), 1057–1065. <https://doi.org/10.1039/b515623h>.
- (20) Weigend, F.; Ahlrichs, R. Balanced Basis Sets of Split Valence, Triple Zeta Valence and Quadruple Zeta Valence Quality for H to Rn: Design and Assessment of Accuracy. *Phys. Chem. Chem. Phys.* **2005**, *7* (18), 3297–3305. <https://doi.org/10.1039/b508541a>.
- (21) Dolg, M.; Wedig, U.; Stoll, H.; Preuss, H. Energy-adjusted Ab Initio Pseudopotentials for the First Row Transition Elements. *J. Chem. Phys.* **1987**, *86* (2), 866–872. <https://doi.org/10.1063/1.452288>.
- (22) Martin, J. M. L.; Sundermann, A. Correlation Consistent Valence Basis Sets for Use with the Stuttgart-Dresden-Bonn Relativistic Effective Core Potentials: The Atoms Ga-Kr and In-Xe. *J. Chem. Phys.* **2001**, *114* (8), 3408–3420. <https://doi.org/10.1063/1.1337864>.
- (23) Marenich, A. V.; Cramer, C. J.; Truhlar, D. G. Universal Solvation Model Based on Solute Electron Density and on a Continuum Model of the Solvent Defined by the Bulk Dielectric Constant and Atomic Surface Tensions. *J. Phys. Chem. B* **2009**, *113* (18), 6378–6396. <https://doi.org/10.1021/jp810292n>.
- (24) Schreckenbach, G.; Ziegler, T. Density Functional Calculations of NMR Chemical Shifts and ESR G-Tensors. *Theor. Chem. Acc.* **1998**, *99* (2), 71–82. <https://doi.org/10.1007/s002140050306>.
- (25) London, F. Théorie Quantique Des Courants Interatomiques Dans Les Combinaisons Aromatiques. *J. Phys. le Radium* **1937**, *8* (10), 397–409. <https://doi.org/10.1051/jphysrad:01937008010039700>.
- (26) McWeeny, R. Perturbation Theory for the Fock-Dirac Density Matrix. *Phys. Rev.* **1962**, *126* (3), 1028–1034. <https://doi.org/10.1103/PhysRev.126.1028>.
- (27) Ditchfield, R. Self-Consistent Perturbation Theory of Diamagnetism I. A Gauge-Invariant LCAO Method for N.M.R. Chemical Shifts. *Mol. Phys.* **1974**, *27* (4), 789–807. <https://doi.org/10.1080/00268977400100711>.
- (28) Wolinski, K.; Hinton, J. F.; Pulay, P. Efficient Implementation of the Gauge-Independent Atomic Orbital Method for NMR Chemical Shift Calculations. *J. Am. Chem. Soc.* **1990**, *112* (23), 8251–8260. <https://doi.org/10.1021/ja00179a005>.
- (29) Cheeseman, J. R.; Trucks, G. W.; Keith, T. A.; Frisch, M. J. A Comparison of Models for Calculating Nuclear Magnetic Resonance Shielding Tensors. *J. Chem. Phys.* **1996**, *104* (14), 5497–5509. <https://doi.org/10.1063/1.471789>.
- (30) Barone, V. Structure, Magnetic Properties and Reactivities of Open-Shell Species From Density Functional and Self-Consistent Hybrid Methods; 1995; pp 287–334. https://doi.org/10.1142/9789812830586_0008.
- (31) Hoops, S.; Gauges, R.; Lee, C.; Pahle, J.; Simus, N.; Singhal, M.; Xu, L.; Mendes, P.; Kummer, U. COPASI - A COMplex PATHway Simulator. *Bioinformatics* **2006**, *22* (24), 3067–3074. <https://doi.org/10.1093/bioinformatics/btl485>.
- (32) Glendening, E. D.; Badenhop, J. K.; Reed, A. E.; Carpenter, J. E.; Bohmann, J. A.; Morales, C. M.; Karafiloglou, P.; Landis, C. R.; Weinhold, F. NBO 6.0. Theoretical Chemistry Institute, University of Wisconsin, Madison 2013.
- (33) Lu, T.; Chen, F. Multiwfn: A Multifunctional Wavefunction Analyzer. *J. Comput. Chem.* **2012**, *33* (5), 580–592. <https://doi.org/10.1002/jcc.22885>.
- (34) Kelly, C. P.; Cramer, C. J.; Truhlar, D. G. Aqueous Solvation Free Energies of Ions and Ion-Water Clusters Based on an Accurate Value for the Absolute Aqueous Solvation Free Energy of the Proton. *J. Phys. Chem. B* **2006**, *110* (32), 16066–16081. <https://doi.org/10.1021/jp063552y>.
- (35) Altus, K. M.; Love, J. A. The Continuum of Carbon–Hydrogen (C–H) Activation Mechanisms and Terminology. *Commun. Chem.* **2021**, *4* (1), 1–11. <https://doi.org/10.1038/s42004-021-00611-1>.
- (36) Perutz, R. N.; Sabo-Étienne, S.; Weller, A. S. Metathesis by Partner Interchange in σ -Bond Ligands: Expanding Applications of the σ -CAM Mechanism. *Angew. Chem. Int. Ed.* **2022**, *61* (5). <https://doi.org/10.1002/anie.202111462>.
- (37) Bogdanović, V. B.; Kröner, M.; Wilke, G. Olefin Complexes of Nickel(0). *Liebigs Ann. Chem.* **1966**, *669* (1), 1–23. <https://doi.org/10.1002/jlac.19666990102>.
- (38) Jonas, K.; Krüger, C. Alkali Metal-Transition Metal π -Complexes. *Angew. Chem. Int. Ed.* **1980**, *19* (7), 520–537. <https://doi.org/10.1002/anie.198005201>.
- (39) Lamm, K.; Stollenz, M.; Meier, M.; Görls, H.; Walther, D. Binuclear Oxalamidinate Complexes (MePd)₂(Oxam) and Homoleptic Complexes of the Type [(THF)_nLi₄(Me₈)M₂] and [(THF)_nLi₃(Ph₄)M] (M=Pd, Ni). *J. Organomet. Chem.* **2003**, *681* (1–2), 24–36. [https://doi.org/10.1016/S0022-328X\(03\)00528-X](https://doi.org/10.1016/S0022-328X(03)00528-X).
- (40) D’Accriscio, F.; Ohleier, A.; Nicolas, E.; Demange, M.; Thillaye Du Boullay, O.; Saffon-Merceron, N.; Fustier-Boutignon, M.; Rezabal, E.; Frison, G.; Nebra, N.; Mézailles, N. [(Dcpp)Ni(η^2 -Arene)] Precursors: Synthesis, Reactivity, and Catalytic Application to the Suzuki–Miyaura Reaction. *Organometallics* **2020**, *39* (10), 1688–1699. <https://doi.org/10.1021/acs.organomet.9b00834>.
- (41) Oddershede, J.; Larsen, S. Charge Density Study of Naphthalene Based on X-Ray Diffraction Data at Four Different Temperatures and Theoretical Calculations. *J. Phys. Chem. A* **2004**, *108* (6), 1057–1063. <https://doi.org/10.1021/jp036186g>.
- (42) Somerville, R. J.; Borys, A. M.; Perez-Jimenez, M.; Nova, A.; Balcells, D.; Malaspina, L. A.; Grabowsky, S.; Carmona, E.; Hevia, E.; Campos, J. Unmasking the Constitution and Bonding of the Proposed Lithium Nickelate “Li₃NiPh₃(Solv)₃”: Revealing the Hidden C₆H₄ Ligand. *Chem. Sci.* **2022**, *13* (18), 5268–5276. <https://doi.org/10.1039/D2SC01244H>.
- (43) Borys, A. M.; Malaspina, L. A.; Grabowsky, S.; Hevia, E. Towards Hexagonal Planar Nickel: A Dispersion-Stabilised Tri-Lithium Nickelate. *Angew. Chem. Int. Ed.* **2022**, *61*, e202209797. <https://doi.org/10.1002/anie.202209797>.
- (44) Borys, A. M.; Hevia, E. Organolithium Aggregation as a Blueprint to Construct Polynuclear Lithium Nickelate Clusters. *Chem. Commun.* **2023**, *59*, 7032–7035. <https://doi.org/10.1039/D3CC01729J>.
- (45) Borys, A. M.; Hevia, E. New Frontiers in Alkali-Metal Nickelates. *Chimia* **2023**, *77* (4), 242–245. <https://doi.org/10.2533/chimia.2023.242>.

Insert Table of Contents artwork here

